A queueing model of an energy harvesting sensor node with data buffering

— Source link ☒

Eline De Cuypere, Koen De Turck, Dieter Fiems

Institutions: Ghent University, CentraleSupélec

Published on: 01 Feb 2018 - Telecommunication Systems (Springer US)

Topics: Mobile wireless sensor network, Wireless sensor network, Key distribution in wireless sensor networks, Sensor node and Energy harvesting

Related papers:

- Stochastic modelling of energy harvesting for low power sensor nodes

- Optimal data collection in wireless sensor networks with correlated energy harvesting

- An Analytical Approach to the Design of Energy Harvesting Wireless Sensor Nodes

- Energy Buffer Dimensioning Through Energy-Erlangs in Spatio-Temporal-Correlated Energy-Harvesting-Enabled Wireless Sensor Networks

- Transmission Policies for Energy Harvesting Sensors with Time-Correlated Energy Supply

Share this paper: ☐ ☐ ☐ ☐

A queueing model of an energy harvesting sensor node with data buffering

Eline De Cuypere[1], Koen De Turck[2], and Dieter Fiems[1]

[1] Ghent University, Department TELIN
Sint-Pietersnieuwstraat 41, B-9000 Ghent, Belgium.

[2] CentraleSupélec, L2S
Gif-sur-Yvette, France.

May 8, 2017

Abstract

Battery lifetime is a key impediment to long-lasting low power sensor nodes and networks thereof. Energy harvesting — conversion of ambient energy into electrical energy — has emerged as a viable alternative to battery power. Indeed, the harvested energy mitigates the dependency on battery power and can be used to transmit data. However, unfair data delivery delay and energy expenditure among sensors remain important issues for such networks. We study performance of sensor networks with mobile sinks: a mobile sink moves towards the transmission range of the different static sensor nodes to collect their data. We propose and analyse a Markovian queueing system to study the impact of uncertainty in energy harvesting, energy expenditure, data acquisition and data transmission. In particular, the energy harvesting sensor node is described by a system with two queues, one queue corresponding to the battery and the other to the data buffer. We illustrate our approach by numerical examples which show that energy harvesting correlation considerably affects performance measures like the mean data delay and the effective data collection rate.

1 Introduction

Sensor networks, formed by collections of intercommunicating sensor nodes (SN), are used to collect and monitor spatially distributed data like temperature, humidity, movement, noise, etc [1–3]. Sensor networks have a variety of applications including military, environmental, home and health applications, see e.g. Akyildiz et. al [1, 2] for an extensive overview of actual applications and Alemdar and Ersoy [4] for specific applications in healthcare.

A typical SN includes a sensing subsystem, local data processing capability and a data communication subsystem, all drawing power from an on-board battery [5, 6]. As the lifetime of the sensor network mostly depends on the limited energy budget of its SNs, energy conservation has been a major concern in the design of sensor networks since their inception. Indeed, the replacement of batteries is often expensive if not impossible once the SNs are deployed. According to Anastasi et al. [7], controlling the communication subsystem is the key to reducing energy consumption. Ideally, the communication subsystem should be switched off when not needed and waken up again when necessary. This basic idea is applied when operating under dynamic power management (DPM). DPM can be integrated into the medium access control (MAC) protocol or may be implemented independently. A detailed explanation of both approaches with a list of low duty cycle MAC protocols and independent sleep/wakeup protocols are respectively given in section 4.2 and 4.3 of [7].

Despite vast improvements on power consumption and ongoing developments in power management, the limited energy budget of on-board batteries remains an impediment for long-lasting sensor networks. To mitigate or overcome this dependency on batteries, current research effort focusses on the development of sensors that scavenge the necessary energy from their environment [6, 8–12]. This alternative technique is

called energy harvesting (EH). The specific nature of such energy-harvesting wireless sensor networks (EH-WSNs) requires a thorough understanding of the energy harvesting dynamics and its impact on performance.

The present paper studies the performance of a specific type of EH-WSNs: sensor networks where the data is collected by mobile sinks. Such a network consists of static sensors responsible for sensing environmental variables, and mobile sinks that move to designated sink locations where they gather the data that is collected by the static sensors. Sink mobility in conventional sensor networks is known to reduce the energy consumption of the sensors, balance the workload among sensors and overcome the hot-spot effect, and prolong the lifetime of the sensor network [13–21]. Some applications of WSNs with mobile sinks include monitoring of agricultural areas [22], improving WSN data delay in emergency situations [23], and continuous object tracking [24]. Contributions on models for EH-WSNs are discussed below.

1.1   Related literature

Various authors have proposed models for EH-WSNs. Within the control community, Sharma et al. [25] study the optimal energy consumption of an EH-WSN that periodically transmits data. The authors mainly tackle existence questions. In particular, they show the existence of an α-discount optimal and average cost optimal control policy assuming finite energy storage capacity. The same control problem is addressed by Yang and Ulukus [26], albeit in a deterministic setting. That is, the authors consider a setting where the amount of harvested energy and the data arrivals are known in advance. Also in a deterministic setting, Tutuncuoglu and Yener [27] consider optimal transmission policies for short-term throughput maximisation and for transmission completion time minimisation. In contrast, Ozel and Ulukus [28] assume that the amount of energy in consecutive time slots constitutes a sequence of independent random variables and derive the optimal power allocation that maximises the average throughput based on the concepts of information theory. The authors further provide a geometric interpretation for the resulting power allocation. Rajesh et al. [29] find the Shannon capacity of a sensor node with an energy harvesting source and show that the capacity achieving policies are related to throughput optimal policies. They also obtain the capacity when energy conserving sleep-wakeup modes are supported as well as the achievable rate for a system with inefficiencies in energy storage. Finally, Zhang and Seyedi [30] derive the overall probability of packet loss in the network due to channel errors or lack of energy in the nodes. Based on this result, a near-optimal design for sizing a sensor's energy storage and harvesting components is obtained.

Sensors being autonomous in deciding which information to transmit as well as when to transmit, various authors propose game theoretic models; see e.g. [31] for power control games in wireless networks. Tsuo et al. [32] consider a Bayesian game where each node knows its local energy state. An evolutionary hawk and dove game with harvesting nodes transmitting either at high or low power is studied in [33] and [34]. With a focus on solar power, Niyato et al. [35] determined the optimal energy management of sensor nodes adopting a sleep-wakeup strategy by means of a bargaining game.

Other authors propose Markovian models to study EH-WSNs. In particular, Jornet and Akyildiz [36] and Seyedi and Sikdar [37, 38] analyse the battery dynamics of a sensor node as a Markovian model. More precisely, the battery is modeled as a Markovian buffer. Ventura and Chowdhury [39] propose a similar model for an energy harvesting body sensor network and allow for multiple sensor nodes harvesting from the same energy source. Ho et al. [40] and Lee et al. [41] verify statistically that a Markov modulated arrival process is appropriate for describing solar energy harvesting. Sahu et al. [5] study stochastic stability of an energy harvesting node with data buffering and rely on simulation to assess its performance. Michelusi et al. [42] focus on transmission policies for harvesting sensor nodes. Energy harvesting is modelled by a two-state discrete time Markov chain. In [43], battery degradation is studied assuming a Markovian harvesting process with a finite number of states. With battery degradation, the harvested energy is not available perpetually (or till it is consumed), but only remains available for a geometrically distributed amount of time. Finally, Michelusi et al. [44] investigate transmissions when the state of the battery is not known perfectly. In such a scenario, energy outage — a lack of energy to complete the requested transmission — should be taken into account.

Finally, some authors particularly study EH-WSNs with mobile sinks, most authors focussing on optimising the path of the mobile sink or the transmission rate. Ren and Liang [45] formulate an optimisation problem to find an optimal close trajectory for the mobile sink and to schedule the sojourn time at each sojourn location such that the network throughput is maximised. The same authors also study the path

optimisation problem where the path of the mobile sink is constrained [46]. In contrast to optimising the mobile sink path, Ren, Liang and Xu [47] and Mehrabi and Kim [48] focus on optimising the transmission rates when the mobile sink travels along a fixed path with a fixed speed.

1.2 Contribution

The major contributions of this paper are as follows. We propose a versatile Markovian model for an energy-harvesting sensor node in a sensor network where data is collected by a mobile sink. The model allows for introducing correlation in the data collection and energy harvesting processes as well as for introducing differences in energy expenditure while transmitting and/or collecting data. While the Markovian setting at hand allows for computationally efficient performance evaluation of the EH-WSN, it is not limiting in terms of versatility. Indeed, the introduction of a Markovian environment variable allows for the introduction of time-correlation in both energy harvesting and data collection (cfr. infra). We show that various performance measures of interest like the mean data delay, the data collection rate and the mean battery level can be calculated efficiently. By means of illustration, we study the effect of correlation in energy harvesting and sensing on these performance measures and show that time correlation of the energy harvesting process is a key determinant of the performance of the sensor network.

The model at hand primarily focusses on a static node in isolation which senses changes of environmental parameters, its data being collected by a mobile sink. However, the model is sufficiently versatile to be of use in other application scenarios where the randomness of sensing and harvesting have a considerable impact on the performance of the WSN. For example, the model can be used to study nodes that relay data from other sensor nodes to the mobile sink. Indeed, from a modelling perspective, there is no difference in buffering sensed or relayed data.

The present work most closely relates to the Markovian models above. However, in contrast to existing literature, we explicitly account for data buffering. This makes the problem more complex as the energy harvesting sensor node now consists of two buffers: a finite-capacity buffer modelling the battery and an infinite-capacity buffer which tracks the temporarily stored data. From a methodological perspective, the model under study relates to paired queueing systems. Pairing means that transmission is only possible if both queues are nonempty. These systems have been studied in various contexts including leaky-bucket access control [49,50], kitting processes [51,52] and decoupling buffers in production systems [53]. The present paper extends our preliminary findings presented in [54] which also studies an energy harvesting sensor node, but adopts a simplified energy expenditure model.

1.3 Paper organisation

The remainder of this paper is organised as follows. In the next section, the EH-WSN model under investigation and the notational conventions are introduced. In section 3, the stochastic process at hand is shown to fit the framework of quasi-birth-and-death processes (QBD). This section also discusses the numerical solution methodology that leads to the relevant performance measures. To illustrate our approach, section 4 considers various numerical examples. Finally, conclusions are drawn in section 5.

2 Model description

Noting that a battery operates very much like a queue — energy chunks being the "customers" in the queue, see [55, 56] — we focus on a single energy-harvesting sensor node in an WSN as depicted in Figure 1. The energy harvesting sensor node is modelled as a queueing system with two queues, one finite-capacity queue for the battery and one infinite-capacity queue for the data buffer while service is only available when the mobile sink is in range. More precisely, data transmission is only possible when (i) there is sufficient energy, (ii) there is sensed data available and (iii) the mobile sink is within range. The stochastic processes that describe data collection and storage, energy harvesting and storage, energy expenditure and transmissions are described below.

Concerning data acquisition, we assume that the sensor picks up data in accordance with a Markovian arrival process with finite state space $\mathcal{A} = \{a_1, \ldots, a_A\}$. Let Ω_A^1 and Ω_A^0 denote the generator matrices governing state transitions with and without data packet arrivals when the energy queue is not empty.
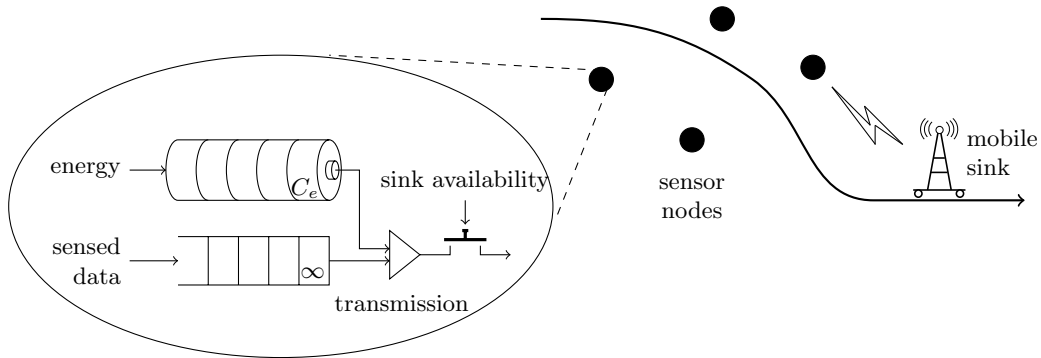
Figure 1: Stochastic model of energy harvesting for low power sensor nodes.

Similarly, let $\widetilde{\Omega}_A^1$ and $\widetilde{\Omega}_A^0$ denote the generator matrices governing state transitions with and without data packet arrivals when the energy queue is empty. Prior to transmission, sensed data is temporarily stored in the data buffer which has infinite capacity. Hence, the data process is described by two state variables: the number of data packets in the buffer and the state of the Markovian arrival process.

Remark 1. We do not exclude the possibility of data arrivals when there is no energy. This is e.g. possible if harvesting always supplies sufficient energy for sensing. In such a case, we can directly subtract the energy for sensing from the harvested energy. The excess energy is then stored in the energy buffer, to be used for transmissions later on.

Remark 2. Here and in the remainder, we assume that generator matrices only collect the transmission rates. Hence, the diagonal elements of the generator matrices of unmarked transmissions like Ω_A^0 are zero. Of course marked transmissions without state change are possible such that the diagonal elements of the generator matrices of the marked transitions like Ω_A^1 may be non-zero.

Analogously to the sensing process, energy harvesting is modelled by a Markovian arrival process with state space $\mathcal{E} \doteq \{e_1, \ldots, e_E\}$ in accordance with the findings in [40]. Let Ω_E^1 and Ω_E^0 denote the generator matrices governing the state transitions with and without energy arrivals respectively. The energy queue has finite capacity C_e to reflect limitations in energy storage. We however do not subscribe to the energy chunk paradigm where each customer in the energy queue represents a chunk of energy. Instead, we associate queue content with energy levels, the difference being that a packet transmission does not necessarily requires a complete chunk of energy and that an "energy arrival" corresponds to an increase of the energy level. While our modelling assumptions still allow for considering the battery as a storage for energy chunks, dropping the concept of energy chunks in favour of energy levels enables one to describe the dynamics of large batteries with less Markovian states. This speeds up the computation of the various performance measures without loss of accuracy (cfr. Figure 4 below).

To introduce energy expenditure and transmission, a third marked Markov process is introduced with state space $\mathcal{D} = \{d_1, \ldots, d_D\}$. This Markov process describes the departures from both energy and data queue and its generator matrices therefore depend on wether or not data and energy are available. When both data buffer content and energy level are non-zero, let Ω_D^e, Ω_D^d, Ω_D^{de} and Ω_D^0 denote the generator matrices governing the transitions when the energy level decreases, when there is a data transmission completed, when the energy level decreases and a data transmission is completed and when there is a state transition with neither an energy drop nor a transmission completion respectively. When there is energy available and no data in the buffer, let $\widehat{\Omega}_D^e$ and $\widehat{\Omega}_D^0$ denote the generator matrices governing the transitions when there is a decrease of energy and when there is no decrease of the energy level. Finally, when there is no energy available, data transmission is also not possible. Hence in this case only non-marked state transitions are possible. Let $\widetilde{\Omega}_D$ denote the corresponding generator matrix. The following two examples illustrate the versatility of the introduced marked Markov process above.

Example 1. As a first example, consider an exogenous Markov process which neither depends on queue content nor energy level. Let Ω_D be its generator matrix and let its state space $\mathcal{D}$ be partitioned into two

4

non-overlapping sets $\mathcal{D}_a$ and $\mathcal{D}_b$ with D_a and D_b elements, respectively. The chain describes the availability of a receiver (like a mobile sink): transmissions occur at a rate μ when the chain is in $\mathcal{D}_a$ (when there is data to send) and there are no transmissions while being in $\mathcal{D}_b$. We further assume that the energy buffer depletes at a rate θ_a during data transmission and at a rate θ_b when there is no transmission. In accordance with [38] and [36], energy is required to communicate with other nodes and to sense, compute and store data. This required amount of energy increases during data transmission such that $\theta_a > \theta_b$. In this case, there are no simultaneous departures from the data and energy queue. Hence, we have,

$$\Omega_D^{de} = 0\,.$$

While there is data and energy, the depletion rates of data and energy queues depend on the state of the exogenous Markov process,

$$\Omega_D^d = \begin{bmatrix} \mu\mathbf{I}_a & 0 \\ 0 & 0 \end{bmatrix}\,, \quad \Omega_D^e = \begin{bmatrix} \theta_a\mathbf{I}_a & 0 \\ 0 & \theta_b\mathbf{I}_b \end{bmatrix}\,,$$

where $\mathbf{I}_a$ and $\mathbf{I}_b$ are identity matrices of size $D_a \times D_a$ and $D_b \times D_b$, respectively. In the absence of data there are no data transmissions such that,

$$\widehat{\Omega}_D^e = \theta_b\mathbf{I}_D\,,$$

with $\mathbf{I}_D$ the identity matrix of size $D \times D$. Finally, as the state of the Markov chain changes independently of the presence of data and energy, we have,

$$\Omega_D^0 = \widehat{\Omega}_D^0 = \widetilde{\Omega}_D = \Omega_D\,.$$

Example 2. Adopting the energy chunk paradigm, assume that every data transmission requires a single energy chunk from the battery, while sensing does not take energy (see Remark 2). Hence, only simultaneous departures from both data and energy queue are possible. This implies $\Omega_D^e = \Omega_D^d = \widehat{\Omega}_D^e = \widehat{\Omega}_D^e = 0$. Adopting the exogenous Markov process with generator matrix Ω_D from the preceding example, state changes of this Markov process do not depend on the presence of data and energy such that,

$$\Omega_D^0 = \widehat{\Omega}_D^0 = \widetilde{\Omega}_D = \Omega_D\,.$$

Again assuming that transmissions occur at a rate μ when the chain is in $\mathcal{D}_a$ and that there are no transmissions while being in $\mathcal{D}_b$, the remaining generator matrix Ω_D^{de} then has the block matrix representation,

$$\Omega_D^{de} = \begin{bmatrix} \mu\mathbf{I}_a & 0 \\ 0 & 0 \end{bmatrix}\,.$$

3 Analysis

We now show that the Markov process at hand is a quasi-birth-death-process (QBD) by identifying the level and phases of the QBD. We first introduce the balance equations as well as some auxiliary matrices.

3.1 Balance equations

Let $Q(t)$ and $C(t)$ be the number of packets and the energy level at time t. Moreover, let $E(t)$, $A(t)$ and $D(t)$ be the state of the energy, data, and transmission process, respectively. The state (in the Markov sense) of the sensor node at time t can then be represented by the vector $[Q(t), C(t), E(t), A(t), D(t)] \in \mathbb{N} \times \mathcal{C} \times \mathcal{E} \times \mathcal{A} \times \mathcal{D}$ with $\mathcal{C} = \{0, 1, \ldots, C_e\}$.

Let $\pi(n, m, e, a, d)$ denote the probability that there are n data packets in the data buffer, that the energy level is m and that the energy, arrival and departure states equal e, a, and d, respectively. In the remainder, let the rate $\omega_X^x(i,j)$ be the (i,j)th element of the matrix Ω_X^x for $X \in \{A, E, D\}$ and for $x \in \{0, 1, d, de, e\}$. The rates $\widehat{\omega}_X^x(i,j)$ and $\widetilde{\omega}_X^x(i,j)$ are defined likewise.

We have the following possible transitions from state (n, m, e, a, d):

- Harvesting: For $m < C_e$, there is an energy arrival with rate $\omega_E^1(e, e')$ for all $e' \in \mathcal{E}$. The new state is $(n, m+1, e', a, d)$. Furthermore, the state of the arrival process changes with rate $\omega_E^0(e, e')$ to state (n, m, e', a, d) for all $e' \in \mathcal{E} \setminus \{e\}$.
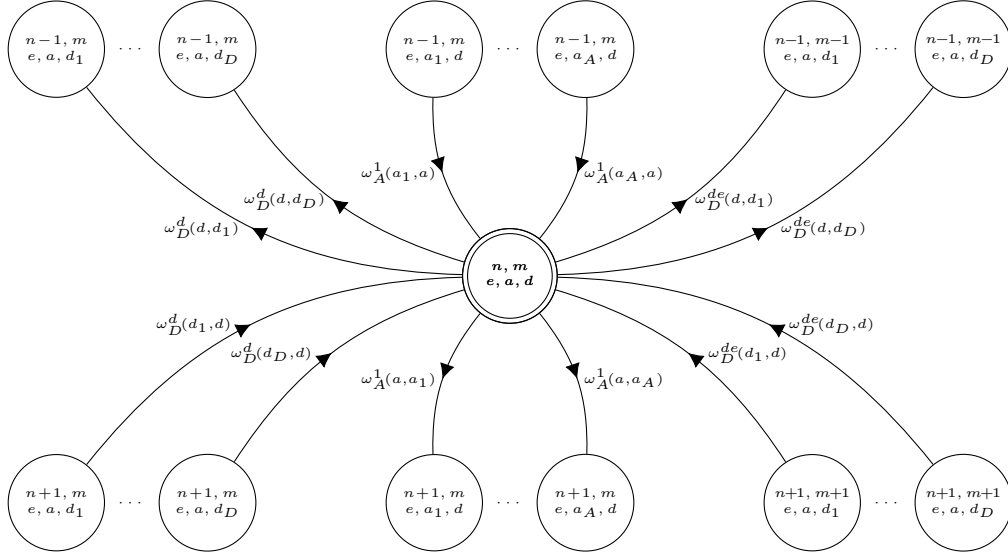
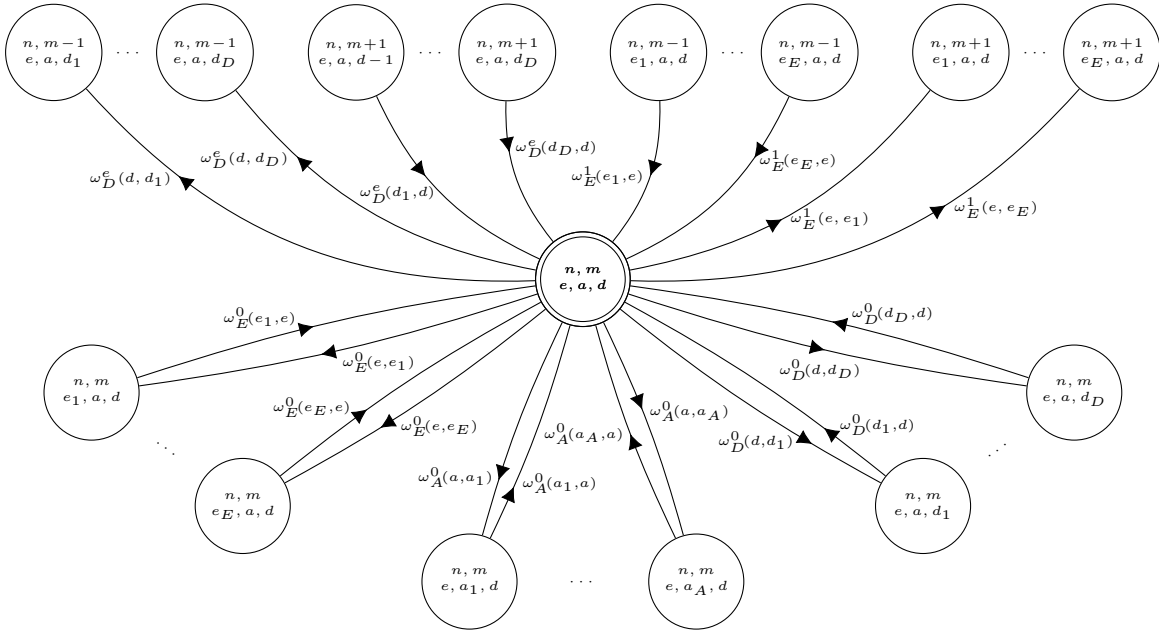Figure 2: Transition rates from and to state (n, m, e, a, d) to and from states in levels $n-1$ and $n+1$.

Figure 3: Transition rates from (to) state (n, m, e, a, d) to (from) states in level n.

- Data acquisition: For $m > 0$ there is a data arrival with rate $\omega_A^1(a, a')$ for $a' \in \mathcal{A}$. The new state is $(n+1, m, e, a', d)$. For $m = 0$ there is a data arrival with rate $\widetilde{\omega}_A^1(a, a')$ for $a' \in \mathcal{A}$. The new state is $(n+1, 0, e, a', d)$. Furthermore, the state of the arrival process changes with rate $\omega_A^0(a, a')$ to state (n, m, e, a', d) for $m > 0$ and with rate $\widetilde{\omega}_A^0(a, a')$ to state $(n, 0, e, a', d)$ for $m = 0$ and for all $a' \in \mathcal{A} \setminus \{a\}$.

- Departures: For $m > 0$ and $n > 0$ there is a simultaneous departure of energy and data with rate $\omega_D^{de}(d, d')$ for $d' \in \mathcal{D}$. The new state is $(n-1, m-1, e, a, d')$. For $m > 0$ and $n > 0$ there is a departure of energy with rate $\omega_D^e(d, d')$ for $d' \in \mathcal{D}$, the new state is $(n, m-1, e, a, d')$. For $m > 0$ and $n > 0$ there is a departure of data with rate $\omega_D^d(d, d')$ for $d' \in \mathcal{D}$, the new state is $(n-1, m, e, a, d')$. For $m > 0$ and $n > 0$ the state of the departure process changes with rate $\omega_D^0(d, d')$ for $d' \in \mathcal{D} \setminus \{d\}$, the new state is (n, m, e, a, d'). For $n = 0$ and $m > 0$, there is a departure of energy with rate $\widehat{\omega}_D^e(d, d')$ for $d' \in \mathcal{D}$, the new state is $(n, m-1, e, a, d')$. For $n = 0$ and $m > 0$ the state of the departure process changes with rate $\widehat{\omega}_D^0(d, d')$ for $d' \in \mathcal{D} \setminus \{d\}$, the new state is (n, m, e, a, d'). Finally, for $m = n = 0$, the state of the departure process changes with rate $\widetilde{\omega}_D^0(d, d')$ for $d' \in \mathcal{D} \setminus \{d\}$, the new state is (n, m, e, a, d').

The possible state transitions from and to state (n, m, e, a, d) (for $n > 0$ and $C > m > 0$) are also depicted in figures 2 and 3. Figure 2 shows the possible transitions that change the size of the data buffer (or the level, cfr. infra), while figure 3 shows the possible transitions where the size of the data buffer does not change. In view of the transition diagrams depcited in Figures 2 and 3 and in view of the possible state transitions described above, we find the following balance equations,

$$\pi(n, m, e, a, d)\gamma(n, m, e, a, d) = \sum_{e' \in \mathcal{E} \setminus \{e\}} \pi(n, m, e', a, d)\omega_E^0(e', e) + \sum_{e' \in \mathcal{E}} \pi(n, m-1, e', a, d)\omega_E^1(e', e)$$

$$+ \mathbb{1}_{\{m>0\}} \sum_{a' \in \mathcal{A} \setminus \{a\}} \pi(n, m, e, a', d)\omega_A^0(a', a) + \mathbb{1}_{\{m>0\}} \sum_{a' \in \mathcal{A}} \pi(n-1, m, e, a', d)\omega_A^1(a', a))$$

$$+ \sum_{a' \in \mathcal{A} \setminus \{a\}} \pi(n, 0, e, a', d)\widetilde{\omega}_A^0(a', a) + \sum_{a' \in \mathcal{A}} \pi(n-1, 0, e, a', d)\widetilde{\omega}_A^1(a', a)$$

$$+ \sum_{d' \in \mathcal{D}} (\mathbb{1}_{\{n>0\}}\pi(n, m+1, e, a, d')\omega_D^e(d', d) + \mathbb{1}_{\{m>0\}}\pi(n+1, m, e, a, d')\omega_D^d(d', d) + \pi(n+1, m+1, e, a, d')\omega_D^{de}(d', d))$$

$$+ \mathbb{1}_{\{m>0, n>0\}} \sum_{d' \in \mathcal{D} \setminus \{d\}} \pi(n, m, e, a, d')\omega_D^0(d', d) + \sum_{d' \in \mathcal{D}} \pi(0, m+1, e, a, d')\widehat{\omega}_D^e(d, d')$$

$$+ \mathbb{1}_{\{m>0\}} \sum_{d' \in \mathcal{D} \setminus \{d\}} \pi(0, m, e, a, d')\widehat{\omega}_D^0(d', d) + \sum_{d' \in \mathcal{D} \setminus \{d\}} \pi(n, 0, e, a, d')\widetilde{\omega}_D(d', d), \quad (1)$$

for $n \in \mathbb{N}$, $m \in \mathcal{C}$, $a \in \mathcal{A}$, $e \in \mathcal{E}$ and $d \in \mathcal{D}$. Here $\gamma(n, m, e, a, d)$ denotes the total outgoing rate from state (n, m, e, a, d),

$$\gamma(n, m, e, a, d) = \sum_{e' \in \mathcal{E} \setminus \{e\}} (\omega_E^0(e, e') + \omega_E^1(e, e')) + \mathbb{1}_{\{m<C_e\}}\omega_E^1(e, e) + \sum_{a' \in \mathcal{A} \setminus \{a\}} \omega_A^0(a, a') + \sum_{a' \in \mathcal{A}} \omega_A^1(a, a')$$

$$+ \mathbb{1}_{\{m>0, n>0\}} \sum_{d' \in \mathcal{D}} (\omega_D^e(d, d') + \omega_D^d(d, d') + \omega_D^{de}(d, d')) + \mathbb{1}_{\{m>0, n>0\}} \sum_{d' \in \mathcal{D} \setminus \{d\}} \omega_D^0(d, d')$$

$$+ \mathbb{1}_{\{m>0, n=0\}} \sum_{d' \in \mathcal{D}} \widehat{\omega}_D^e(d, d') + \mathbb{1}_{\{m>0, n=0\}} \sum_{d' \in \mathcal{D} \setminus \{d\}} \widehat{\omega}_D^0(d, d') + \mathbb{1}_{\{m=0\}} \sum_{d' \in \mathcal{D} \setminus \{d\}} \widetilde{\omega}_D(d, d'). \quad (2)$$

We now focus on the block matrix representation of this system of equations and its numerical solution.

3.2 Auxiliary matrices

We first describe the transition matrices of the marked Markov process that tracks all state information except the queue content and the energy level. Recall that the state space of the energy harvesting process, of the sensor data arrival process and of the departure process are denoted by $\mathcal{E}$, $\mathcal{A}$ and $\mathcal{D}$, respectively. This Markov chain then has state space $\mathcal{K} = \mathcal{E} \times \mathcal{A} \times \mathcal{D}$ with size $K = EAD$ and its transition matrices depend

on the presence of data and energy. Let $\mathbf{I}_E$, $\mathbf{I}_A$ and $\mathbf{I}_D$ denote identity matrices with size $E \times E$, $A \times A$ and $D \times D$, respectively. In the remainder we use the symbol $\otimes$ to denote the Kronecker product.

- When both energy level and queue content are non-zero, the unmarked transitions (when there are neither arrivals nor departures) are governed by the $K \times K$ matrix,

$$\mathbf{A} = \Omega_E^0 \otimes \mathbf{I}_A \otimes \mathbf{I}_D + \mathbf{I}_E \otimes \Omega_A^0 \otimes \mathbf{I}_D + \mathbf{I}_E \otimes \mathbf{I}_A \otimes \Omega_D^0 \,.$$

  Analogously, when there is energy but no data and when there is neither energy nor data, the unmarked transitions are governed by the $K \times K$ matrices,

$$\widehat{\mathbf{A}} = \Omega_E^0 \otimes \mathbf{I}_A \otimes \mathbf{I}_D + \mathbf{I}_E \otimes \Omega_A^0 \otimes \mathbf{I}_D + \mathbf{I}_E \otimes \mathbf{I}_A \otimes \widehat{\Omega}_D^0 \,.$$

  and,

$$\widetilde{\mathbf{A}} = \Omega_E^0 \otimes \mathbf{I}_A \otimes \mathbf{I}_D + \mathbf{I}_E \otimes \widetilde{\Omega}_A^0 \otimes \mathbf{I}_D + \mathbf{I}_E \otimes \mathbf{I}_A \otimes \widetilde{\Omega}_D \,,$$

  respectively.

- The $K \times K$ matrix $\mathbf{B}_E$ governs the transitions when there is an arrival in the battery:

$$\mathbf{B}_E = \Omega_E^1 \otimes \mathbf{I}_A \otimes \mathbf{I}_D \,.$$

- The $K \times K$ matrices $\mathbf{B}_A$ and $\widetilde{\mathbf{B}}_A$ govern the transitions when there is an arrival in the data buffer and there is energy and no energy respectively:

$$\mathbf{B}_A = \mathbf{I}_E \otimes \Omega_A^1 \otimes \mathbf{I}_D \,, \quad \widetilde{\mathbf{B}}_A = \mathbf{I}_E \otimes \widetilde{\Omega}_A^1 \otimes \mathbf{I}_D \,.$$

- The marked transitions when the energy level drops and/or when there is a transmission again depend on the presence of data and energy. When there is both data and energy, let $\mathbf{C}_D$, $\mathbf{C}_E$ and $\mathbf{C}_{DE}$ denote the $K \times K$ generator matrices governing the transitions when there is a transmission, an energy drop or both, respectively:

$$\mathbf{C}_D = \mathbf{I}_E \otimes \mathbf{I}_A \otimes \Omega_D^d \,,$$
$$\mathbf{C}_E = \mathbf{I}_E \otimes \mathbf{I}_A \otimes \Omega_D^e \,,$$
$$\mathbf{C}_{DE} = \mathbf{I}_E \otimes \mathbf{I}_A \otimes \Omega_D^{de} \,.$$

  When there is energy but no data, the $K \times K$ matrix governing the transitions when the energy level decreases is given by,

$$\widehat{\mathbf{C}}_E = \mathbf{I}_E \otimes \mathbf{I}_A \otimes \widehat{\Omega}_D^e \,.$$

Remark 3. In the remainder, all results will be expressed in terms of the matrices defined above. These results remain valid when the arrival processes of data and energy and the departure process are correlated as well. In that case there is a single marked Markov process, with marks for data arrivals, energy arrivals and data transmissions.

3.3 Quasi-birth-death process

The Markov process under study is a homogeneous quasi-birth-and-death process (QBD), see [57]. A Markov process is a QBD if its state can be described by a positive integer *level* and a *phase* taking values in a finite set such that there are only transitions within the same level or to neighbouring levels. The generator of such a Markov process has a block tridiagonal structure, which allows for efficiently calculating various performance measures of the Markov process (cfr. infra).

In the present setting, the level or block index indicates the number of data packets available while the phase, i.e. the index within a block element, indicates both the battery level and the state of the modulating chain. That is, the phase takes values in the set $\mathcal{C} \times \mathcal{K}$. Describing the state of the system by the triplet $[n, m, i]$, $n \in \mathbb{N}$ being the number of data packets available, $m \in \mathcal{C}$ being the battery level and $i \in \mathcal{K}$ being the state of the modulating chain, the balance equations show that there are only transitions restricted to states

in the same level (from state $[n, *, *]$ to state $[n, *, *]$) or between two adjacent levels (from state $[n, *, *]$ to state $[n+1, *, *]$ or state $[n-1, *, *]$).

We then find that the generator matrix of the Markov chain has the following block matrix representation,

$$
\mathcal{Q} = \begin{bmatrix}
\mathcal{B}_0 & \mathcal{A}_2 & 0 & 0 & \cdots \\
\mathcal{A}_0 & \mathcal{A}_1 & \mathcal{A}_2 & 0 & \cdots \\
0 & \mathcal{A}_0 & \mathcal{A}_1 & \mathcal{A}_2 & \cdots \\
0 & 0 & \mathcal{A}_0 & \mathcal{A}_1 & \cdots \\
\vdots & \vdots & \vdots & \vdots & \ddots
\end{bmatrix}.
\tag{3}
$$

The blocks are matrices of size $P \times P$ with $P \doteq (C_e + 1)K$ and are given by,

$$
\mathcal{B}_0 = \begin{bmatrix}
\widetilde{\mathbf{A}} & \mathbf{B}_E & 0 & \cdots & 0 \\
\widehat{\mathbf{C}}_E & \widehat{\mathbf{A}} & \mathbf{B}_E & \cdots & 0 \\
0 & \widehat{\mathbf{C}}_E & \widehat{\mathbf{A}} & \cdots & 0 \\
\vdots & \vdots & \vdots & \ddots & \vdots \\
0 & 0 & 0 & \cdots & \widehat{\mathbf{A}}
\end{bmatrix},
\tag{4}
$$

$$
\mathcal{A}_0 = \begin{bmatrix}
0 & 0 & \cdots & 0 & 0 \\
\mathbf{C}_{DE} & \mathbf{C}_D & \cdots & 0 & 0 \\
0 & \mathbf{C}_{DE} & \cdots & 0 & 0 \\
\vdots & \vdots & \ddots & \vdots & \vdots \\
0 & 0 & \cdots & \mathbf{C}_{DE} & \mathbf{C}_D
\end{bmatrix},
\tag{5}
$$

$$
\mathcal{A}_1 = \begin{bmatrix}
\widetilde{\mathbf{A}} & \mathbf{B}_E & 0 & \cdots & 0 \\
\mathbf{C}_E & \mathbf{A} & \mathbf{B}_E & \cdots & 0 \\
0 & \mathbf{C}_E & \mathbf{A} & \cdots & 0 \\
\vdots & \vdots & \vdots & \ddots & \vdots \\
0 & 0 & 0 & \cdots & \mathbf{A}
\end{bmatrix},
\tag{6}
$$

and,

$$
\mathcal{A}_2 = \begin{bmatrix}
\widetilde{\mathbf{B}}_A & 0 & 0 & \cdots & 0 \\
0 & \mathbf{B}_A & 0 & \cdots & 0 \\
0 & 0 & \mathbf{B}_A & \cdots & 0 \\
\vdots & \vdots & \vdots & \ddots & \vdots \\
0 & 0 & 0 & \cdots & \mathbf{B}_A
\end{bmatrix}.
\tag{7}
$$

Having defined the different blocks of the QBD process, we now focus on the solution method. Recall that the state of the Markov chain is described by the triplet $[n, m, i]$; n is the size of the data buffer, m is the size of the battery and i is the state of the modulating chain. Let $\pi(n, m, i)$ be the steady state probability to be in state $[n, m, i]$ and let $\boldsymbol{\pi}$ be the vector with elements $\pi(n, m, i)$. The vector $\boldsymbol{\pi}$ satisfies the balance equations,

$$
\boldsymbol{\pi}(\mathcal{Q} - \partial\mathcal{Q}) = 0.
$$

Here, for any matrix $\mathcal{X}$, we define $\partial\mathcal{X}$ to be the diagonal matrix with diagonal elements equal to the row sums of $\mathcal{X}$. A well-known method for finding the stationary distribution of QBD processes is the matrix-geometric method. Using the vector notation $\boldsymbol{\pi}_n = [\pi(n, m, i)]_{m \in \mathcal{C}, i \in \mathcal{K}}$, the matrix geometric method shows that these probability vectors can be expressed as,

$$
\boldsymbol{\pi}_n = \boldsymbol{\pi}_0 \mathbf{R}^n.
\tag{8}
$$

where the so-called $P \times P$ rate matrix $\mathbf{R}$ is the minimal non-negative solution of the non-linear matrix equation

$$
\mathbf{R}^2 \mathcal{A}_0 + \mathbf{R}\bar{\mathcal{A}}_1 + \mathcal{A}_2 = \mathbf{0},
$$

with $\bar{\mathcal{A}}_1 = \mathcal{A}_1 - \partial\mathcal{A}_0 - \partial\mathcal{A}_1 - \partial\mathcal{A}_2$. We compute the rate matrix by implementing the improved iterative algorithm of [57, chapter 8, p.179-187]. Once the rate matrix is found, the remaining unknown vector $\boldsymbol{\pi}_o$ is the unique solution of,

$$\boldsymbol{\pi}_0(\mathbf{I}_P - \mathbf{R})^{-1}\mathbf{1}_P = 1\,, \quad \boldsymbol{\pi}_0(\bar{\mathcal{B}}_0 + \mathbf{R}\mathcal{A}_0) = 0\,,$$

with $\bar{\mathcal{B}}_0 = \mathcal{B}_0 - \partial\mathcal{A}_2$, where $\mathbf{I}_P$ is the $P \times P$ identity matrix and where $\mathbf{1}_P$ is a column vector of P ones.

3.4   Performance measures

Once the steady state probabilities have been determined numerically, we can calculate a number of interesting performance measures for the harvesting energy sensor node. For ease of notation, we introduce the marginal probability mass function of the battery level $\pi^{(e)}(m)$ and of the data buffer content $\pi^{(d)}(n)$,

$$\pi^{(e)}(m) = \sum_{i \in \mathcal{K}} \sum_{n=0}^{\infty} \pi(n, m, i) = \sum_{n=1}^{\infty} \boldsymbol{\pi}_0 \mathbf{R}^n (\mathbf{e}_m \otimes \mathbf{1}_K) = \boldsymbol{\pi}_0(\mathbf{I}_P - \mathbf{R})^{-1}(\mathbf{e}_m \otimes \mathbf{1}_K)\,,$$

$$\pi^{(d)}(n) = \sum_{i \in \mathcal{K}} \sum_{m=0}^{C_e} \pi(n, m, i) = \boldsymbol{\pi}_0 \mathbf{R}^n \mathbf{1}_P\,.$$

Here $\mathbf{e}_m$ is a column vector of size $C_e + 1$ with all its elements zero, apart from the mth element which is 1, while $\mathbf{1}_K$ is a column vector of K ones. We have the following performance measures.

- The mean data buffer content $\overline{Q}_d$ and the variance of the data buffer content V_d equal

$$\overline{Q}_d = \sum_{n=1}^{\infty} \pi^{(d)}(n)n\,, \quad V_d = \sum_{n=1}^{\infty} \pi^{(d)}(n)n^2 - (\overline{Q}_d)^2\,,$$

  and can be expressed in terms of $\boldsymbol{\pi}_0$ and $\mathbf{R}$ as follows,

$$\overline{Q}_d = \boldsymbol{\pi}_0(\mathbf{I}_P - \mathbf{R})^{-1}\mathbf{R}(\mathbf{I}_P - \mathbf{R})^{-1}\mathbf{1}_P\,,$$

$$V_d = 2\boldsymbol{\pi}_0(\mathbf{I}_P - \mathbf{R})^{-1}\mathbf{R}(\mathbf{I}_P - \mathbf{R})^{-1}\mathbf{R}(\mathbf{I}_P - \mathbf{R})^{-1}\mathbf{1}_P + \overline{Q}_d - \overline{Q}_d^2\,.$$

- We express the battery level as a fraction of the maximum capacity of the battery. The mean battery level $\overline{B}_e$ and its variance V_e are given by,

$$\overline{B}_e = \sum_{m=1}^{C_e} \pi^{(e)}(m)\frac{m}{C_e}\,, \quad V_e = \sum_{m=1}^{C_e} \pi^{(e)}(m)\frac{m^2}{C_e^2} - (B_e)^2\,.$$

- The mean data delay $\overline{D}$ (calculated based on Little's theorem) is the average amount of time between the arrival of a data packet and its transmission:

$$\overline{D} = \frac{\overline{Q}_d}{a_d}\,.$$

  Here a_d is the data collection rate: the mean number of data packets that are sensed per time unit. The data collection rate a_d only accounts for packets that effectively enter the data buffer. Its value can be determined by the following expression,

$$a_d = \boldsymbol{\pi}_0(\mathbf{I}_P - \mathbf{R})^{-1}\mathcal{A}_2\mathbf{1}_P\,.$$

4   Numerical results

Having established the model and its numerical analysis, we now evaluate the performance of an energy harvesting sensor node that is visited by a mobile sink. Assuming no simultaneous departures from the data and energy queue during data transmission, the numerical experiments fit Example 1 of Section 2.

We consider a scenario in which an isolated sensor is visited by a mobile sink for a fraction of the time. We make the following assumptions:

- Sensing and transmissions are only possible when there is energy (the battery level exceeds 0).

- The battery depletes at a rate θ_a during data transmission and at a rate θ_b when there is no transmission.

- To analyse the impact of irregularity in the energy harvesting process, we assume that energy arrives in accordance with an interrupted Poisson arrivals. The interrupted Poisson process considered here is a two-state Markovian process. In the active state, energy arrives in accordance with a Poisson process with rate λ_e^* whereas no new energy arrives in the inactive state. Let α_e and β_e denote the rate from the active to the inactive state and vice versa, respectively. For convenience, we use the more intuitive parametrisation $(\sigma_e, \kappa_e, \lambda_e)$, with

$$\sigma_e = \frac{\beta_e}{\alpha_e + \beta_e}, \quad \kappa_e = \frac{1}{\alpha_e} + \frac{1}{\beta_e}, \quad \lambda_e = \lambda_e^* \sigma_e.$$

  Here, σ_e is the fraction of time in which the interrupted Poisson process is active, the time scale parameter κ_e is the average duration of an active and an inactive period, and λ_e is the arrival load of harvested energy.

- Also data arrives in accordance with a (two-state) interrupted Poisson process. In the active state, data arrives in accordance with a Poisson process with rate λ_d^* whereas no new data arrives in the inactive state. Let α_d and β_d denote the rate from the active to the inactive state and vice versa, respectively. For convenience, we use the more intuitive parametrisation $(\sigma_d, \kappa_d, \lambda_d)$, with

$$\sigma_d = \frac{\beta_d}{\alpha_d + \beta_d}, \quad \kappa_d = \frac{1}{\alpha_d} + \frac{1}{\beta_d}, \quad \lambda_d = \lambda_d^* \sigma_d.$$

  where σ_d is the fraction of time during which the interrupted Poisson process is active, the time scale parameter κ_d is the average duration of an active and an inactive period, and λ_d is the arrival load of harvested energy.

- Data transmission times are exponentially distributed with service rate $\mu = 1$.

- The fraction of time in which the mobile sink is available (unavailable) is exponentially distributed with mean $1/\alpha_t$ $(1/\beta_t)$ such that the fraction of time σ_r the mobile sink is available and the average duration κ_t of an available and non-available period equals

$$\sigma_t = \frac{\beta_t}{\alpha_t + \beta_t}, \quad \kappa_t = \frac{1}{\alpha_t} + \frac{1}{\beta_t}.$$

  Note that $1/\alpha_t$ is the mean time that the mobile sink is in the transmission range of the sensor node. In a scenario where the mobile sink does not stop, but only passes by with speed v, the mean time in range relates to the transmission range T of the sensor node as T/v.

We can now study the effects of correlation in energy harvesting and data collection. However, we first evaluate the choice of C_e which we will use in the remainder of this section. The value of C_e corresponds to the number of energy levels we account for. The more levels one accounts for, the more accurate we can capture the state of the battery. However, more levels also means that the number of possible phases of the QBD increases which leads to longer calculation times, the number of phases being equal to $P = 8(C_e + 1)$ with the assumptions above. Fortunately, it turns out that once we have a sufficiently large C_e, a further increase hardly influences the performance measures. Hence, there is no need to further increase C_e beyond this level.

To determine the value of C_e, Figure 4 depicts the cumulative distribution function of the (normalised) battery level for different values of C_e, κ_e and the normalised harvesting rate $\widehat{\lambda}_e$ as indicated. Normalisation of the battery levels means that battery level C_e corresponds to 100% and the normalised harvesting rate $\widehat{\lambda}_e$ is the harvesting rate that is needed to completely load the battery in the same time, but when the battery has 100 levels. The normalised depletion rates $\widehat{\theta}_a$ and $\widehat{\theta}_b$ are defined likewise. The corresponding rates for a model with capacity C_e are then calculated as follows,

$$\lambda_e = \widehat{\lambda}_e \frac{C_e}{100}, \quad \theta_a = \widehat{\theta}_a \frac{C_e}{100}, \quad \theta_b = \widehat{\theta}_b \frac{C_e}{100}.$$
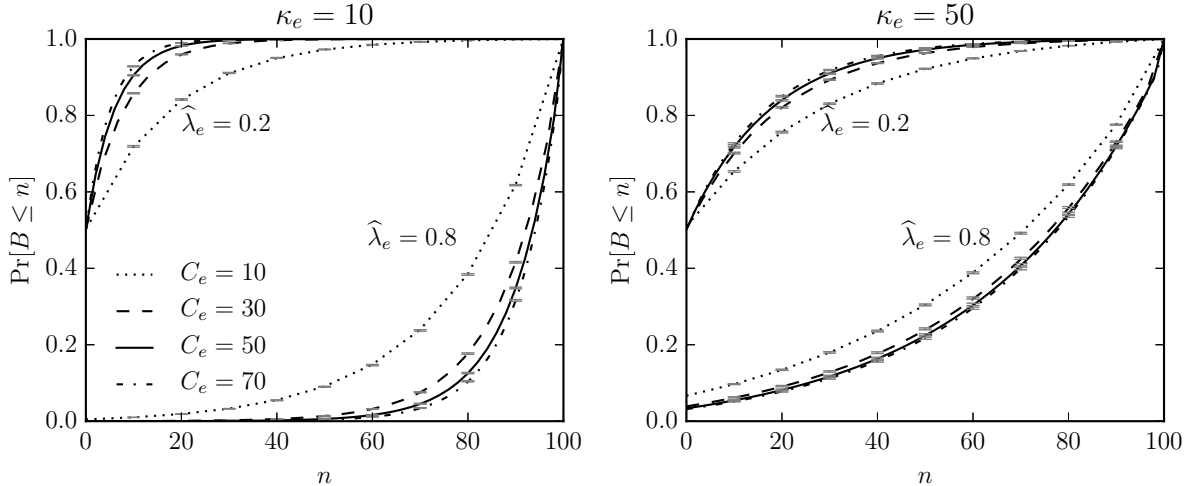
Figure 4: Cumulative distribution of the (normalised) battery level for different values of C_e, κ_e and $\widehat{\lambda}_e$ as indicated. (Energy collection $\sigma_e = 0.1$; Poisson data arrivals with rate $\lambda_d = 0.001$; energy depletion rates $\widehat{\theta}_a = 1.6$ and $\widehat{\theta}_b = 0.4$; mobile sink parameters $\sigma_t = 0.01$ and $\kappa_t = 1000$.)

It is easily checked that the average time to completely deplete or load the battery is equal for every choice of C_e. We assume the following depletion rates: $\widehat{\theta}_a = 1.6$ and $\widehat{\theta}_b = 0.4$. We further assume Poisson data arrivals with rate $\lambda_d = 0.001$, the mobile sink is available for a fraction $\sigma_t = 0.01$ of the time, with $\kappa_t = 1000$, while the node collects energy for a fraction $\sigma_e = 0.1$ of the time. Different values of $\widehat{\lambda}_e$ and κ_e are assumed as indicated.

Figure 4 shows that the cumulative distribution function for $C_e = 50$ hardly differs from the corresponding curve for $C_e = 70$. Therefore, we will fix the number of battery levels to $C_e = 50$ in the remainder. For this choice, the number of phases (and therefore also the size of the matrices) equals $P = 408$. Figure 4 further reveals that the probability mass is either concentrated around battery level 0 (for $\widehat{\lambda}_e = 0.2$) or around battery level C_e (for $\widehat{\lambda}_e = 0.4$). This observation is in line with queueing theory: for finite queues most of the probability mass of the queue content is either concentrated near 0 when the load is below the service capacity or near full capacity when this is not the case.

Remark 4. In figure 4 as well as in the following figures we also depict simulation results for a number of points on all curves to verify the correctness of our calculations. To simulate the system at hand, we have used uniformisation to simulate the time-evolution of the Markov chain directly from the balance equations (1) and (2), see [59, p. 61]. The simulation generates (i) samples from the energy level and (ii) samples from the data delay. The delay is calculated by logging the arrival times of all data arrivals such that we can calculate the data delay upon departure. In addition, for every arrival we generate an arrival indicator sample which equals one if the arrival is admitted and zero if this is not the case. Recall that a data arrival is not admitted if there is no energy. We have simulated 10^8 samples from the system state to estimate the mean and distribution of the battery level, 2×10^6 data delay samples to estimate the mean delay, and 2×10^6 arrival indicator samples to estimate the fraction of admitted arrivals. We have used the batch means method to estimate the confidence interval of these estimators.

Having decided on the number of battery levels, we now study the effect of energy harvesting correlation. Figure 5 depicts the mean data delay $\overline{D}$, the mean battery level $\overline{B}_e$ and the fraction of arriving data that is collected $\phi_d = a_d/\lambda_d$ versus the arrival rate λ_e of energy packets for different values of κ_e as indicated. Note that the sensor may not be able to collect all data as data is only collected if there is energy. The sensor node harvests during a fraction $\sigma_e = 0.1$ of the time. In addition, data arrives in accordance with a Poisson process with rate $\lambda_d = 0.001$ whereas the mobile sink is with the sensor node 1% of the time ($\sigma_t = 0.01$) and returns after a time $\kappa_t = 1000$ on average. Finally, the depletion rate of the battery during transmission is 4
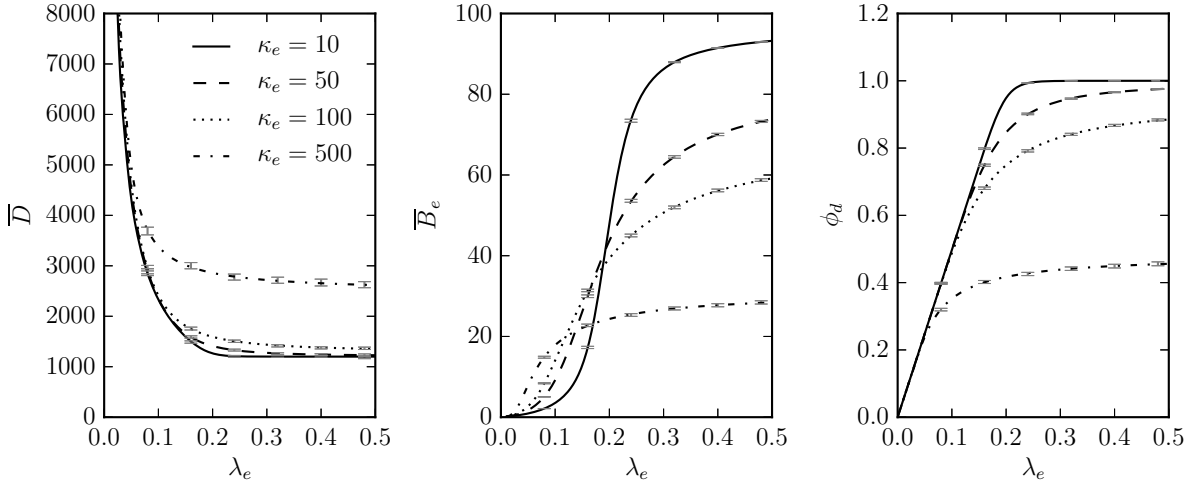
12

Figure 5: Mean data delay $\overline{D}$, mean battery level $\overline{B}_e$ and data collection rate ϕ_d vs. the energy arrival rate λ_e for different values of κ_e. (Energy collection parameters $\sigma_e = 0.1$; Poisson data arrivals with rate $\lambda_d = 0.001$; energy depletion rates $\theta_a = 0.8$ and $\theta_b = 0.2$; battery capacity $C_e = 50$; availability of the mobile sink $\sigma_t = 0.01$ and $\kappa_t = 1000$.)

times the depletion rate while it is not transmitting ($\theta_a = 0.8$ and $\theta_b = 0.2$) while the battery has $C_e = 50$ levels in accordance with the findings of Figure 4.

From Figure 5 we observe that when there arrives more energy (increasing λ_e), the mean data delay decreases, the mean battery level increases and the fraction of data that is sensed increases as well. This is not unexpected. When there is more energy, it is less likely that the sensor node runs out of energy when the mobile sink passes by. If the sensor node has no energy, transmissions need to be postponed till the next time the mobile sink passes by such that the data delay increases. Moreover, if there is more excess energy, more energy will be stored in the battery such that the mean battery level increases. Finally, when there is more energy, the chance to run out of energy decreases such that it is less likely that the sensor node is without energy when there is something to sense.

We further observe that the mean data delay is considerably higher for higher κ_e while the amount of sensed data is considerably lower for higher κ_e. Higher κ_e (for a fixed σ_e) means that we have longer periods with harvesting followed by longer periods without harvesting. In other words, the supply of energy is more bursty and the chance to run out of energy during the long periods without harvesting increases. This in turn implies that it is more likely that there cannot be transmissions (an increase of the mean data delay) or sensing (lower ϕ_d) due to a lack of energy. The effect of κ_e on the mean battery level is less clear. For low λ_e, increasing κ_e leads to an increase of the mean battery level while the opposite effect is observed for higher values of λ_e. This effect can be explained by accounting for the finiteness of the battery. For low λ_e it is not likely that energy is lost as the battery is hardly ever fully loaded. In this case, the battery level increases to higher levels during the longer periods with harvesting leading to an overall increase of the mean battery level. In contrast, for higher λ_e, the battery capacity is reached during the longer periods with harvesting and energy is lost. Due to this loss, the battery runs out of energy during the longer periods without harvesting, leading to an overall decrease of the mean battery level. Results not shown here confirm these qualitative effects for different values of σ_t, κ_t and different θ_a and θ_b as well as for interrupted Poisson data arrivals.

The effect of κ_e on $\overline{D}$, $\overline{B}_e$ and ϕ_d is further investigated in Figure 6 which depicts these performance measures versus κ_e for different values of λ_e as indicated. We retain the assumptions on the various parameter values from Figure 5 apart from the Poisson data arrivals. We now consider interrupted Poisson data arrivals with parameters $\lambda_d = 0.001$, $\sigma_d = 0.1$ and $\kappa_d = 100$. The figure shows that the mean data delay increases with κ_e while the fraction of sensed data decreases, in line with the observations of Figure 5. The mean battery level first increases and then decreases, which again can be explained by the finiteness of the battery.
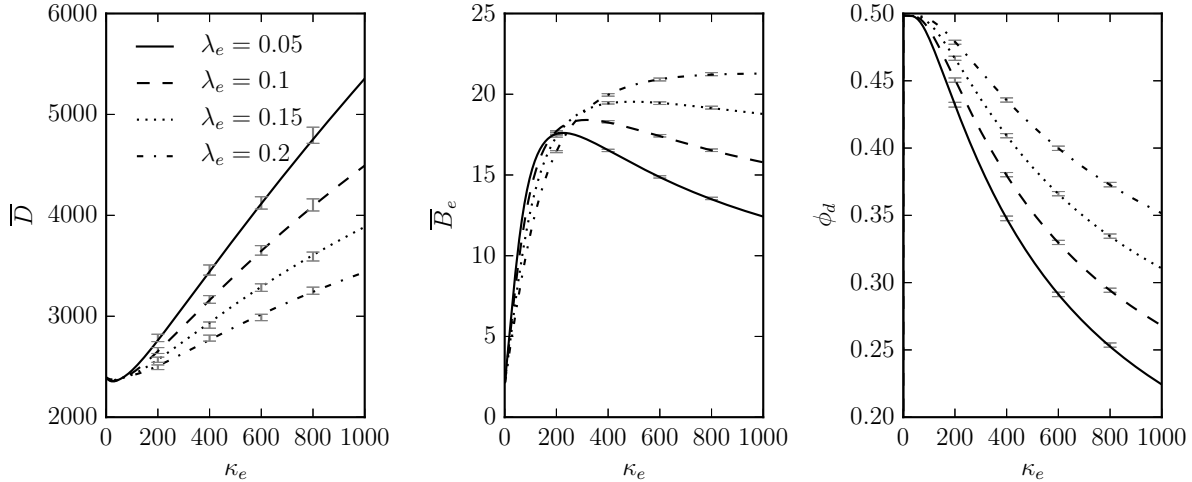
13

Figure 6: Mean data delay $\overline{D}$, mean battery level $\overline{B}_e$ and data collection rate ϕ_d vs. the time scale parameter for for different values of λ_e. (Energy collection parameters $\sigma_e = 0.1$; Interrupted Poisson data arrivals with rate $\lambda_d = 0.001$, and parameters $\sigma_d = 0.1$ and $\kappa_d = 100$; energy depletion rates $\theta_a = 0.8$ and $\theta_b = 0.2$; battery capacity $C_e = 50$; mobile sink availability parameters $\sigma_t = 0.01$ and $\kappa_t = 1000$.)

For low values of κ_e, an increase results in longer periods where the battery builds up (during harvesting) followed by longer periods where it builds down (without harvesting) which implies an increase of the queue content. For even larger κ_e, energy loss during the harvesting becomes more likely (even for fairly low λ_e), this energy loss resulting in lower battery levels. Notice that the reduction in energy expenditure (less data is sensed as seen on the ϕ_d plot, so less data needs to be transmitted), cannot compensate this energy loss.

In contrast to harvesting correlation which affects $\overline{D}$, $\overline{B}_e$ and ϕ_d, changing the time scale of the visits by the mobile sink only affects the mean data delay. Figure 7 depicts the mean data delay $\overline{D}$, the mean battery level $\overline{B}_e$ and the fraction of arriving data that is collected $\phi_d = a_d/\lambda_d$ versus the arrival rate λ_e of energy packets for different values of κ_t as indicated. We use the parameter values of Figure 5 for the data arrival process, the battery capacity, the energy expenditure and the availability of the mobile sink and further assume $\kappa_e = 50$. It is readily seen that an increase of κ_t results in longer data delays. This is not unexpected as the time between consecutive visits of the mobile sink increases. In contrast, it is not entirely expected that κ_t hardly influences $\overline{B}_e$ and $\overline{\phi}_d$. To visualise the limited effect of κ_t, we have plotted the deviation of $\overline{B}_e$ and ϕ_d with respect to the case $\kappa_t = 1$: $\overline{B}_e^* = \overline{B}_e(\kappa_t)/\overline{B}_e(1) - 1$, $\phi_d^* = \phi_d(\kappa_t)/\phi_d(1) - 1$. Additional experimentation with different values of κ_e, σ_e, κ_t and σ_t confirmed this qualitative observation.

Finally, we study the effect of correlation in the sensing process. Figure 8 depicts the mean data delay $\overline{D}$, the mean battery level $\overline{B}_e$ and the fraction of arriving data that is collected $\phi_d = a_d/\lambda_d$ versus the arrival rate λ_e of energy packets for different values of κ_d as indicated. We use the parameter values of Figure 5 for the battery capacity, the energy expenditure and the parameters of the mobile sink and further assume $\kappa_e = 50$ and $\lambda_d = 0.001$. The value of κ_d hardly influences $\overline{W}$, $\overline{B}_e$ and $\overline{\phi}_d$. To visualise the limited effect of κ_d on $\overline{B}_e$ and $\overline{\phi}_d$, we have plotted the deviation of $\overline{B}_e$ and ϕ_d with respect to the case that the arrival process is Poisson. Qualitatively similar results were obtained when we increased and decreased κ_t and σ_t which indicates that the arrival correlation of sensing data is not detrimental to performance.

5   Conclusion

In this paper, we analysed the performance of an energy harvesting sensor node assuming uncertainty in energy harvesting, energy depletion and data acquisition. To this end, energy harvesting sensor nodes were modelled as stochastic systems with two queues: one queue representing the battery and one queue representing a sensor data buffer. We investigated EH-WSNs where data is collected by a mobile sink which
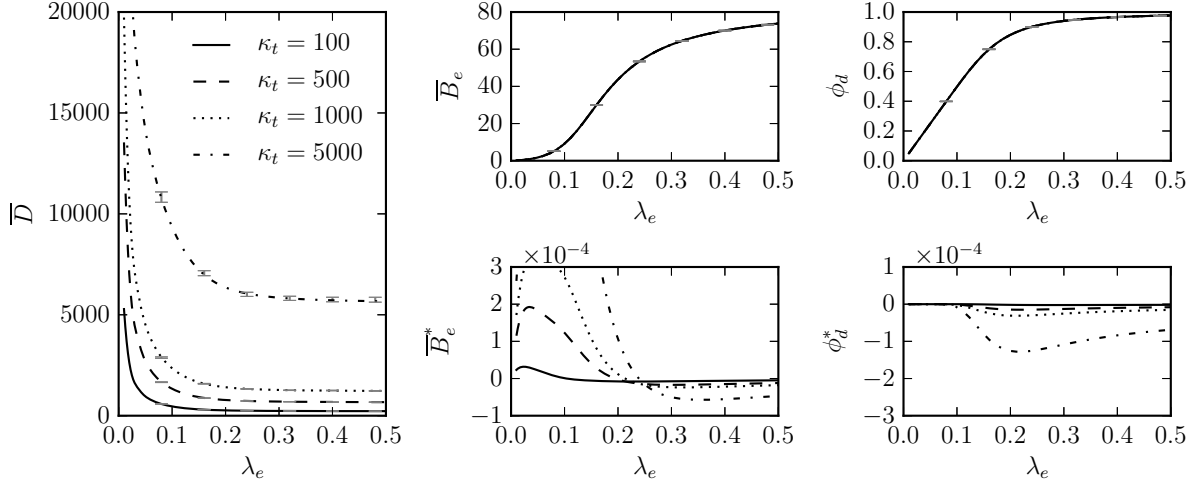
14

Figure 7: Mean data delay $\overline{D}$, mean battery level $\overline{B}_e$ and data collection rate ϕ_d vs. the energy arrival rate λ_e for different values of κ_t. (Energy collection fraction $\sigma_e = 0.1$; Poisson data arrivals with rate $\lambda_d = 0.001$; energy depletion rates $\theta_a = 0.8$ and $\theta_b = 0.2$; battery capacity $C_e = 50$; collection parameters $\sigma_t = 0.01$ and $K_t = 1000$.)
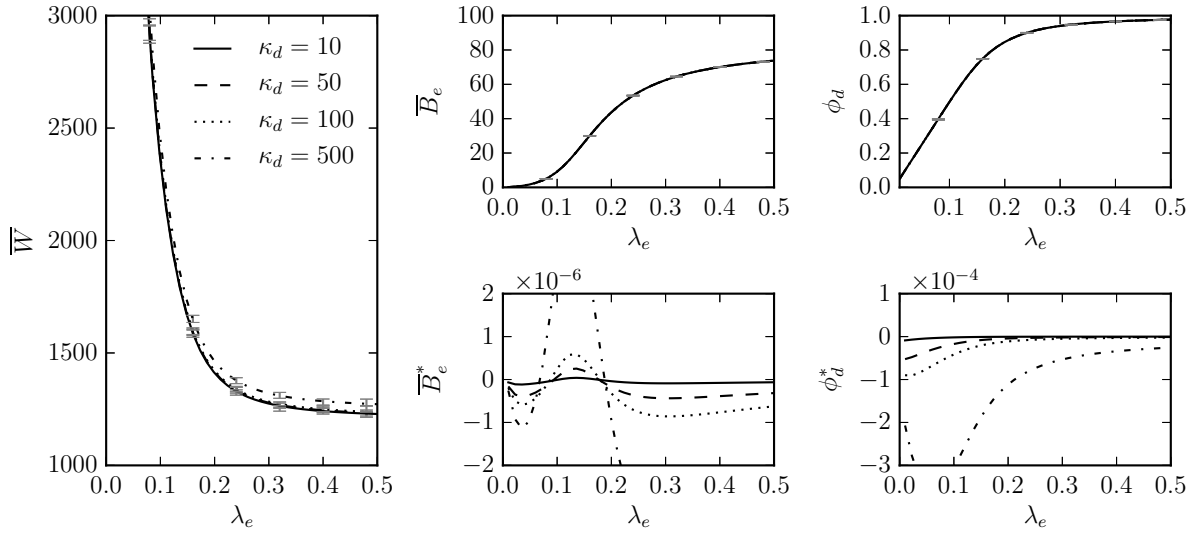

Figure 8: Mean data delay $\overline{D}$, mean battery level $\overline{B}_e$ and data collection rate ϕ_d vs. the energy arrival rate λ_e for different values of κ_d. (Energy collection fraction $\sigma_e = 0.1$ and $\kappa_e = 50$; Interrupted Poisson data arrivals with $\sigma_d = 0.1$, with rate $\lambda_d = 0.001$ and with κ_d as indicated; energy depletion rates $\theta_a = 0.8$ and $\theta_b = 0.2$; battery capacity $C_e = 50$; collection parameters $\sigma_t = 0.01$ and $K_t = 1000$.)

15

introduced an additional source of uncertainty as sensor nodes can only send data when the mobile sink is in range. Methodologically, we showed that the queueing system at hand can be described by a homogeneous quasi-birth-death process (QBD). This allowed for calculating various performance measures computationally efficient by means of matrix-geometric methods. Extensive numerical experimentation revealed that time correlation of the harvesting process is a key determinant of the performance of the EH-WSN. In contrast, the time between visits of the mobile sink only affected the mean data delay, whereas data arrival correlation had only limited impact on all performance measures.

References

[1] I.F. Akyildiz, W. Su, Y. Sankarasubramaniam, E. Cayirci. Wireless sensor networks: a survey. *Computer Networks* 38(4):393–422, 2002.

[2] I.F. Akyildiz, M.C. Vuran. *Wireless sensor networks.* Wiley, 2010.

[3] Y.K. Tan, S.K. Panda. Review of Energy Harvesting Technologies for Sustainable Wireless Sensor Network. In: *Sustainable Wireless Sensor Network*, Chapter 2. INTECH, 2010.

[4] H. Alemdar, C. Ersoy. Wireless sensor networks for healthcare: A survey. *Computer Networks* 54(15):2688–2710 , 2010.

[5] A. Sahu, E.B. Fernandez, M. Cardei, M. Vanhilst. A pattern for a sensor node. In: Proceedings of the 17th conference on Pattern Languages of Programs, 2010.

[6] S. Sudevalayam, P. Kulkarni. Energy Harvesting Sensor Nodes: Survey and Implications. *IEEE Communications Surveys & Tutorials* 13:443–461, 2011.

[7] G. Anastasi, M. Conti, M. Di Francesco, A. Passarella. Energy conservation in wireless sensor networks: a survey. *Ad Hoc Networks* 7:537–568, 2009.

[8] J.A. Paradiso, T. Starner. Energy scavenging for mobile and wireless electronics. *IEEE Pervasive Computing* 4:18–27, 2005.

[9] D. Gunduz , K. Stamatiou, N. Michelusi, M. Zorzi. Designing intelligent energy harvesting communication systems *IEEE Communications Magazine* 52(1):210–216, 2014.

[10] X. Lu, P. Wang, D. Niyato, D.I. Kim, Z. Han. Wireless Networks With RF Energy Harvesting: A Contemporary Survey. *IEEE Communications Surveys & Tutorials* 17(2):757–789, 2015.

[11] C. Yang, K. Chin. On Nodes Placement in Energy Harvesting Wireless Sensor Networks for Coverage And Connectivity. *IEEE Transactions on Industrial Informatics* 13(1):27–36, 2017.

[12] F. Yang, L. Du, W.G. Chen, J. Li, Y.Y. Wang, D.S. Wang. Hybrid energy harvesting for condition monitoring sensors in power grids *Energy* 118:435–445, 2017.

[13] Y. Bi, J. Niu, L. Sun, W. Huangfu and Y. Sun. Moving Schemes for Mobile Sinks in Wireless Sensor Networks. *IEEE International Performance Computing, and Communications Conference.* pp. 101–108, 2007.

[14] M. Di Francesco, S.K. Das, G. Anastasi. Data collection in wireless sensor networks with mobile elements: A survey. *ACM Transactions on Sensor Networks* 8(1):1–31, 2011.

[15] S. Gao, H. Zhang, S.K. Das. Efficient data collection in wireless sensor networks with path-constrained mobile sinks. *IEEE Transactions on Mobile Computing* 10(4):592–608, 2011.

[16] D. Turgut, L. Bölöni. Heuristic approaches for transmission scheduling in sensor networks with multiple mobile sinks. *The Computer Journal* 54(3):332–344, 2009.

[17] Y. Yun, Y. Xia. Maximizing the lifetime of wireless sensor networks with mobile sink in delay-tolerant applications. *IEEE Transactions on Mobile Computing* 9:1308–1318, 2010.

[18] W. Liang, J. Luo, X. Xu. Prolonging network lifetime via a controlled mobile sink in wireless sensor networks. In: Proc of the IEEE Global Communications Conference (GLOBECOM), Miami, Florida, 2010.

[19] W. Liang, J. Luo. Network lifetime maximization in sensor networks with multiple mobile sinks. In: Proc. of the IEEE Conference on Local Computer Networks (LCN), Bonn, Germany, 2011.

[20] A. Kaswan, K. Nitesh, J.K. Prasanta. Energy efficient path selection for mobile sink and data gathering in wireless sensor networks. *AEU-International Journal of Electronics and Communications* 73:110–118, 2017.

[21] C. Wang, S. Guo, T. Yang. An Optimization Framework for Mobile Data Collection in Energy-Harvesting Wireless Sensor Networks IEEE Transactions on Mobile Computing 15(12):2969–2986, 2016.

[22] T.H.F. Khan, D.S. Kumar. Mobile collector aided energy reduced (MCER) data collection in agricultural wireless sensor networks. In: Proc. of the 6th IEEE International Conference on Advanced Computing. pp. 629–633, 2016.

[23] T.T. Truong, K.N. Brown, C.J. Sreenan. Using mobile sinks in wireless sensor networks to improve building emergency response. In: Proc. of the Royal Irish Academy Research. Colloquium on Wireless as an Enabling Technology, 2010.

[24] C. Kim, H. Cho, S. Kim, T. Yang, S.H. Kim. Sink Mobility Support Scheme for Continuous Object Tracking in Wireless Sensor Networks 30th IEEE International Conference on Advanced Information Networking And Applications . pp. 452–457, 2016.

[25] V. Sharma, U. Mukherji, V. Joseph. Optimal energy management policies for energy harvesting sensor nodes. *IEEE Transactions on Wireless Communications* 6:1326–1336, 2010.

[26] J. Yang, S. Ulukus. Optimal Packet scheduling in an Energy Harvesting Communication System. *IEEE Transactions on Communications* 60(1):220–230, 2012.

[27] K. Tutuncuoglu, A. Yener. Optimum Transmission Policies for Battery Limited Energy Harvesting Nodes. *IEEE Transactions on Wireless Communications* 11:1180–1189, 2012.

[28] O. Ozel, S. Ulukus. Information-theoretic analysis of an energy harvesting communication system, In: Proc. of the 21st IEEE International Symposium on Personal, Indoor and Mobile Radio Communications, Istanbul, Turkey, 26-30 Sept. 2010, pp. 330–335.

[29] R. Rajesh, V. Sharma, P. Viswanath. Information capacity of Energy harvesting, In: Proc. of the 2011 IEEE International Symposium on Information Theory, St. Petersburg, Russia, 31 July-5 Aug. 2011, pp. 2363–2367.

[30] S. Zhang, A. Seyedi. Analysis and Design of Energy Harvesting Wireless Sensor Networks with Linear Topology, In: Proc. of the IEEE International Conference on Communications (ICC), Kyoto, Japan, 5-9 June 2011.

[31] F. Meshkati, H.V. Poor, S.C. Schwartz. Energy-Efficient Resource Allocation in Wireless Networks, *IEEE Signal Processing Magazine* 24:58–68, 2007.

[32] F.Y. Tsuo, H.P. Tan, Y.H. Chew, H.Y. Wei. Energy-Aware Transmission Control for Wireless Sensor Networks Powered by Ambient Energy Harvesting: A Game-Theoretic Approach, In: Proc. of the IEEE International Conference on Communications (ICC), Kyoto, Japan, 5-9 June 2011.

[33] E. Altman, D. Fiems, M. Haddad, J. Gaillard. Semi-Dynamic Hawk and Dove Game Applied to Power Control. In: Proc. of the 31st Annual IEEE International Conference on Computer Communications (INFOCOM), 2012.

[34] M. Haddad, E. Altman, J. Gaillard, D. Fiems. A Semi-Dynamic Evolutionary Power Control Game. In: Proc. of Networking 2012, Lecture Notes in Computer Science vol. 7290, 2012, pp 392–403.

[35] D. Niyato, M.M. Rashid, V.K. Bhargave. Wireless sensor networks with energy harvesting technologies: A game-theoretic approach to optimal energy management. *IEEE Wireless Communications* 14:90–96, 2007.

[36] J.S. Jornet, I.F. Akyildiz. Joint Energy Harvesting and Communication Analysis for Perpetual Wireless Nanosensor Networks in the Terahertz Band. *IEEE Transactions on nanotechnology* 11:570–580, 2012.

[37] A. Seyedi, B. Sikdar. Performance modelling of transmission schedulers capable of energy harvesting. In: Proc. of the IEEE International Conference on Communications (ICC), Cape Town, 2010.

[38] A. Seyedi, B. Sikdar. Energy efficient transmission strategies for body sensor networks with energy harvesting, *IEEE Transactions on Communications* 58(7):2116–2126, 2010.

[39] J. Ventura, K. Chowdhury. Markov modelling of energy harvesting body sensor networks, Proceedings of PIMRC, Toronto, 2011, pp.2168–2172.

[40] C.K. Ho, P.D. Khoa, P.C. Ming, Markovian models for harvested energy in wireless communications, In: Proc. of the 10th International Conference on Computational Science, Amsterdam (ICCS), 2010.

[41] P. Lee, Z.A. Eu, M. Han, H. Tan, Empirical modeling of a solar powered energy harvesting wireless sensor node for time-slotted operation. In: Porc of the IEEE Wireless Communications & Networking Conference (WCNC), Cancun, 2011, pp.179–184.

[42] N. Michelusi, K. Stamatiou, M. Zorzi. Transmission Policies for Energy Harvesting Sensors with Time-Correlated Energy Supply. *IEEE Transactions on Communications* 61(7):2988–3001, 2013.

[43] N. Michelusi, L. Badia, R. Carli, L. Corradini, M. Zorzi. Energy Management Policies for Harvesting-Based Wireless Sensor Devices with Battery Degradation. *IEEE Transactions on Communications* 61(12):4934–4947, 2013

[44] N. Michelusi, L. Badia, M. Zorzi. Optimal Transmission Policies for Energy Harvesting Devices With Limited State-of-Charge Knowledge. *IEEE Transactions on Communications* 62(11):3969–3982, 2014.

[45] X. Ren, W. Liang. Delay-Tolerant Data Gathering in Energy Harvesting Sensor Networks With a Mobile Sink. In: Proc of the IEEE Global Communications Conference (GLOBECOM), Anaheim, California, 2012.

[46] X. Ren, W. Liang. The use of a mobile sink for quality data collection in energy harvesting sensor networks. In: IEEE Wireless Communications and Networking Conference. pp. 1145–1150, Shanghai, 2013.

[47] X. Ren, W. Liang, W. Xu. Data Collection Maximization in Renewable Sensor Networks via Time-Slot Scheduling. *IEEE Transactions on Computers* 64(7):1870–1883, 2015.

[48] A. Mehrabi, K. Kim. Maximizing Data Collection Throughput on a Path in Energy Harvesting Sensor Networks Using a Mobile Sink. *IEEE Transactions on Mobile Computing* 15(3):690–704, 2016.

[49] S. Wittevrongel, H. Bruneel. A heuristic analytic technique to calculate the cell loss ration in a leaky bucket with bursty input traffic. *AEUE – International Journal of Electronics and Communications* 48(3):162–169, 1994.

[50] S. Wittevrongel, H. Bruneel. Analytic study of the queueing performance and the departure process of a leaky bucket with bursty input traffic. *AEUE – International Journal of Electronics and Communications* 50(1):1–10, 1996.

[51] E. De Cuypere, K. De Turck, D. Fiems, Performance analysis of a kitting process as a paired queue. *Mathematical Problems in Engineering*, Article ID 843184, http://dx.doi.org/10.1155/2013/843184, 2013.

[52] E. De Cuypere, D. Fiems. Performance evaluation of a kitting process, Proceedings of the 17th International Conference on analytical and stochastic modelling techniques and applications, Lecture Notes in Computer Science, 6751, 2011.

[53] E. De Cuypere, K. De Turck, D. Fiems. Performance analysis of a decoupling stock in a Make-to-Order system. In: Proc. of the 14th IFAC Symposium on Information Control Problems in Manufacturing, Bucharest, Romenia, 2012.

[54] E. De Cuypere, K. De Turck, D. Fiems. Stochastic Modelling of Energy Harvesting for Low Power Sensor Nodes. In: Proc. of the 7th International Conference on Queueing Theory and Network Applications, Kyoto, Japan, 2012.

[55] R. Valentini, N. Dang, M. Levorato, E. Bozorgzadeh. Modeling and control battery aging in energy harvesting systems. In: Proc. of SmartGridComm, pp. 515–520, 2015.

[56] E. Gelenbe, E.T. Ceran. Energy Packet Networks With Energy Harvesting *IEEE Access* 4:1321–1331, 2016.

[57] G. Latouche, V. Ramaswami. *Introduction to Matrix Analytic Methods in Stochastic Modeling*. SIAM, 1999.

[58] G. Latouche, Queues with paired customers. *Journal of Applied Probability* 18:684–696, 1981.

[59] S. Asmussen, P.W. Glynn. Stochastic Simulation: Algorithms and Analysis, Springer, 2007.